KSME

Springer

Journal of Mechanical Science and Technology 35 (12) 2021

Original Article
DOI 10.1007/s12206-021-1135-6

Keywords:
· Laser printing and scanning unit
· F-theta lens
· Aspherical surface
· Optic
· Root mean square
· Peak to valley

Correspondence to:
Zhen Qin
qin@sdut.edu.cn
Sung-Ki Lyu
sklyu@gnu.ac.kr

Citation:
Park, Y.-W., Qin, Z., Lyu, S.-K. (2021). Study on design and processing performance verification of a 600 dpi f-theta lens. Journal of Mechanical Science and Technology 35 (12) (2021) 5643~5653. http://doi.org/10.1007/s12206-021-1135-6

Received May 20th, 2021
Revised July 28th, 2021
Accepted August 30th, 2021

† Recommended by Editor Hyung Wook Park

Study on design and processing performance verification of a 600 dpi f-theta lens

Yong-Woo Park[1], Zhen Qin[2,3] and Sung-Ki Lyu[3]

[1]Department of Convergence Mechanical Engineering, 501, Gyeongsang National University, Jinju-daero, Jinju-si, Gyeongsangnam-do 52828, Korea, [2]School of Mechanical Engineering, Shandong University of Technology, No. 266 West Xincun Road, Zibo 255049, China, [3]School of Mechanical and Aerospace Engineering, 501, Gyeongsang National University, Jinju-daero, Jinju-si, Gyeongsangnam-do 52828, Korea

Abstract With the ever-improving requirements for printing resolution, printing speed and noise, laser printing and scanning unit based on the precision optical technology have been greatly developed in recent years. The f-theta lens is considered to be the most important element in the laser printing and scanning unit that affects the printing resolution, which can convert the computer digital data into a light signal and transmit the optical information to the laser printing and scanning system. It is a mainly composed of a light source, collimator lens, and polygon mirror. Many researches of obtaining the higher printing or scanning resolution by increasing the number of lenses have been studied, but this method will inevitably increase the volume of the entire system. In this study, a solution to optimize the optical performance of the f-theta lens was proposed and verified by a series of optical numerical investigation on the laser printing and scanning unit. The satisfactory optical performance of the optimal f-theta lens is confirmed by experimental method. In addition, the modality of the f-theta lens was verified by injection molding simulation.

1. Introduction

The laser printing and scanning unit of a laser multifunction device plays a role of converting digital data into light information and transferring the digital signals from a computer to the laser printing and scanning unit [1-5]. The core components of a laser printing and scanning unit are composed of the f-theta lens, polygon mirror, cylinder lens, collimator lens, laser diodes, laser control circuit boards, and cases [6-9].

The most important core technology in the laser printing and scanning unit is to transmit the optical dot from the laser diode to the drum through the correct optical path [10-13]. A collimator lens is used to create a parallel beam by preventing the scattering of diffused beam from the laser diode. In order to collect the parallel beam from the collimator to the sub-scanning side on the polygon mirror surface, the light from the cylinder lens is imaged on the polygon mirror surface, then diffuses again and enters the f-theta lens. An f-theta lens is named by the tan value of the beam width and focal length f in the drum due to the polygon mirror angle. One of the most important parts of a laser printing and scanning unit is this f-theta lens. Fig. 1 is a conceptual diagram of the laser printing and scanning unit system. In regards to work undertaken in this field, Nor et al. [14] studied the system design of laser printing and scanning unit A3, Yoo et al. [15] performed the injection molding of the laser printing and scanning unit optical system, Lim et al. [16] performed optical scanning, and Park et al. [17] is researching the numerical analysis for the injection molding of an aspheric lens for a photo pick-up device. Furthermore, Lee et al. [18] is currently working on the effect analysis of birefringence of a plastic f-theta lens on the beam diameter, Lee et al. [19] is conducting research on aspherical surface in the laser writing optics. Many other researchers are continuously researching to improve its performance

Table 1. Specification of laser printing and scanning unit.

No.		Spec.	Remarks
Resolution		600 dpi	
Beam size	Main beam	75+15/-10 μm	
	Sub beam	80+20/-10 μm	
Laser diode	Wave length	785+10/-15 μm	
	Power	0.300 mW ± 0.02 mW	
f-theta lens	Magnification error	Maximum 0.7 %	297 mm
	Part magnification error	Maximum 1.5 %	25.4 mm
Pitch error	Near	Maximum 10 μm	
	All	Maximum 20 μm	
Jitter	Low frequency	Maximum 0.025 %	
	Radio frequency	Maximum 0.012 %	
Scan line property	Bow	Maximum 1 mm	25 °C
	Skew	Maximum 1 mm	
Polygon motor	Voltage	24 V DC±10 %	
	Start current	Maximum 2.0 A	
	Operating current	Maximum 1.0 A	
	Driving method	PWM control	

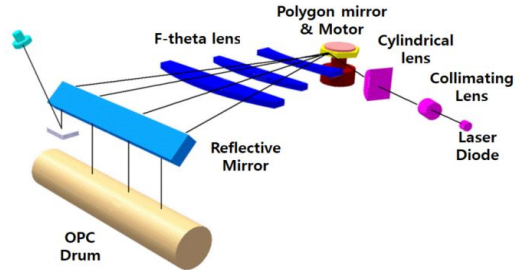

Fig. 1. Laser printing and scanning unit system.

and characteristics [20-27].

In this study, a solution to optimize the optical performance of the f-theta lens was proposed and verified by a series of optical numerical investigation on the laser printing and scanning unit. The satisfactory optical performance of the optimal f-theta lens is confirmed by experimental method. In addition, the modality of the f-theta lens was verified by injection molding simulation.

2. Optical design

2.1 Optical design of laser printing and scanning unit

Table 1 shows the specifications of the optical system of the basic laser printing and scanning unit system.

Fig. 2 shows the positions of the f-theta lens, cylinder lens, collimator lens, polygon mirror, laser diode, etc., which are the main components of the laser scanning unit, and the optical system is a = 80.936 mm, b = 3.798 mm, c = 79.72 mm, d = 12.423 mm, e = 11.926 mm, g = 109.56 mm, h = 34 °, i = 28 °, j = 0.221 mm, k = 4.019 mm, l = 300 mm.

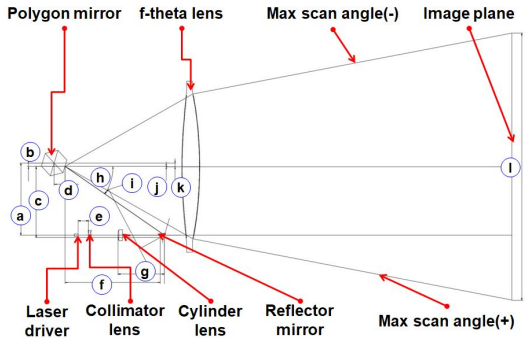

Fig. 2. Layout of laser printing and scanning unit.

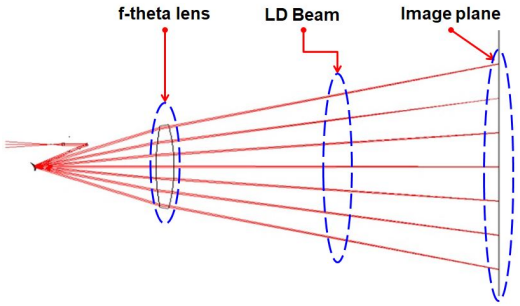

(a) 2D drawing

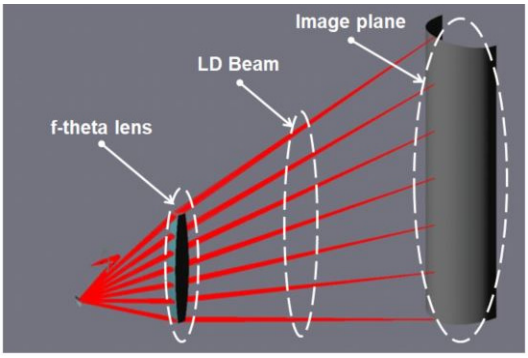

(b) 3D modeling

Fig. 3. Simulation of laser printing and scanning unit.

Fig. 3(a) is a 2D simulation executed based on such an optical system. Fig. 3(b) shows the laser printing and scanning unit in 3D with optical design software (code-V), along with a sample of the beam emitted from the laser diode actually passing through each lens to the image plane. By using beam size it is possible to know which part of the f-theta lens the beam passed through at each location. Using this simulation it is possible to study any problems in a specific part of the f-theta lens. In such a simulation, it was decided to secure the optical design data of the entire laser scanning unit as shown in Table 2.

2.2 Optical design of f-theta lens

The design of the optical system of the laser printing and scanning unit is paramount in order to increase the degree of design freedom, improve the processing characteristics of the

Table 2. Optical design data.

Surface	Type	Y radius [mm]	X radius [mm]	T [mm]	Y aperture [mm]	X aperture [mm]
Object	Sphere	Infinity	Infinity	1	0	0
1	Sphere	Infinity	Infinity	0.29	0.5	0.5
2	Sphere	Infinity	Infinity	12.291	0.5	0.5
3	Asphere	63.4367	63.4367	2.5	1.4445	1.4445
4	Asphere	-8.5035	-8.5035	5.55	1.5919	1.5919
Stop	Sphere	Infinity	Infinity	20	12	4.5
6	Sphere	Infinity	Infinity	-10	1.664	1.664
7	Cylinder	Infinity	-31.32	-3	1.591	1.591
8	Sphere	Infinity	Infinity	-57.8194	1.591	1.591
9	Sphere	Infinity	Infinity	-11.5140	1.5896	1.5896
10	Sphere	Infinity	Infinity	0	5.2274	5.2274
11	Sphere	Infinity	Infinity	12.074	6.036	6.036
12	Sphere	Infinity	Infinity	-12.074	4.6057	4.6057
13	Sphere	Infinity	Infinity	0	11.1549	11.1549
14	Sphere	Infinity	Infinity	11.577	7.7249	7.7249
15	Sphere	Infinity	Infinity	0	2.0781	2.0781
16	Sphere	Infinity	Infinity	134.779	2.0781	2.0781
17	Y toroid	553.3673	-167.9241	20	69.4855	6
18	X toroid	-458.7217	-43.4387	359.242	72.1045	6
Image	Cylinder	Infinity	50	0	297	297

Table 3. Specification of f-theta lens.

Item		Specification	Remarks
Effective scan width		A3 type 297 mm	
Lens number		1 Pcs	Zeonex e48r (cyclo olefin polymer)
Focal length		A3 type 210 mm	
Polygon mirror		Circumscribed circle 30 mm, 6 facet	
Beam size	Main	75 μm, (+15/-10), deviation 20 μm ↓	
	Sub	80 μm, (+20/-10), deviation 30 μm ↓	
Laser wave length		785 nm (+15/-10)	25 °C
Ambient light ratio		80 % ↑	0±100 mm
Magnification error		0.7 % ↓	Scanning outermost
Partial magnification error		1.5 % ↓	Any 1 inch within 297 mm scan width

focusing ability for high resolution, and enable the use of various lens materials. The f-theta lens was designed based on the design and verification data of the optical system for increasing the workability of the lens. Table 3 shows the specifications of the f-theta lens.

Optical design of f-theta lens Eqs. (1)-(4), Eq. (1) indicates the distance between the tangent plane and the aspherical surface on the incident surface, and the value of F (H) is, can

Table 4. Optical design data of effective surface.

Incident surface [mm]		Exit surface [mm]	
Curv1	0.001807118	Cy	-0.00217997
Curv2	-0.005955072	Cx	-0.023020947
Radius1	553.367295328	Radius1	-458.72169859
Radius2	-167.924082194	Radius2	-43.4386995461
K	-1.948401	Ky	-5.442065
A	-0.155366E-08	Kx	-0.952428
B	-0.413175E-11	Ar	-0.228885E-07
C	0.229084E-15	Ap	-0.102777E+01
D	0.467319E-20	Br	-0.709488E-12
		Bp	0.549368E+00
		Cr	-0.241121E-14
		Cp	-0.533682E+00
		Dr	0.144902E-19
		Dp	0.831840E-01

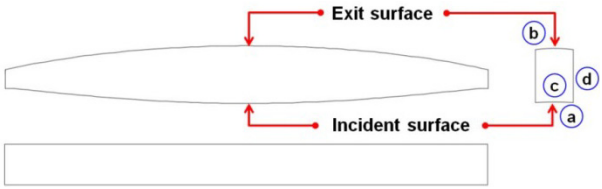

(a) 2D drawing

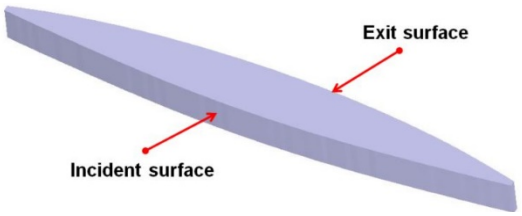

(b) 3D modeling

Fig. 4. Conceptual design of f-theta lens using code-V.

be represented by a value related to the distance from the optical axis to a point on the sphere. Here, Curv1, Curv2, Cx and Cy are a value indicating the radius of curvature. The reason for using only even exponents in the H value is that the aspherical surface is asymmetric with respect to the Z axis. The values of A, B, C and D are equations related to the incident of light, and the coefficients of $(A)H^4$, $(B)H^6$, $(C)H^8$ and $(D)H^{10}$ are values indicating the degree of deformation of the aspherical surface. Eqs. (2) and (3) show the correction values of the previously designed parameters. Eq. (4) shows an aspherical equation with respect to the exit surface. In this way, the f-theta lens was designed through the optical method. The 2D drawing and 3D modeling was established by using the optical design software of code-V. The design parameters used in the calculation can be found in Table 4. The f-theta lens was designed as shown in Figs. 4(a) and (b). Here, a represents the incident surface radius, which value is 167.924 mm; b

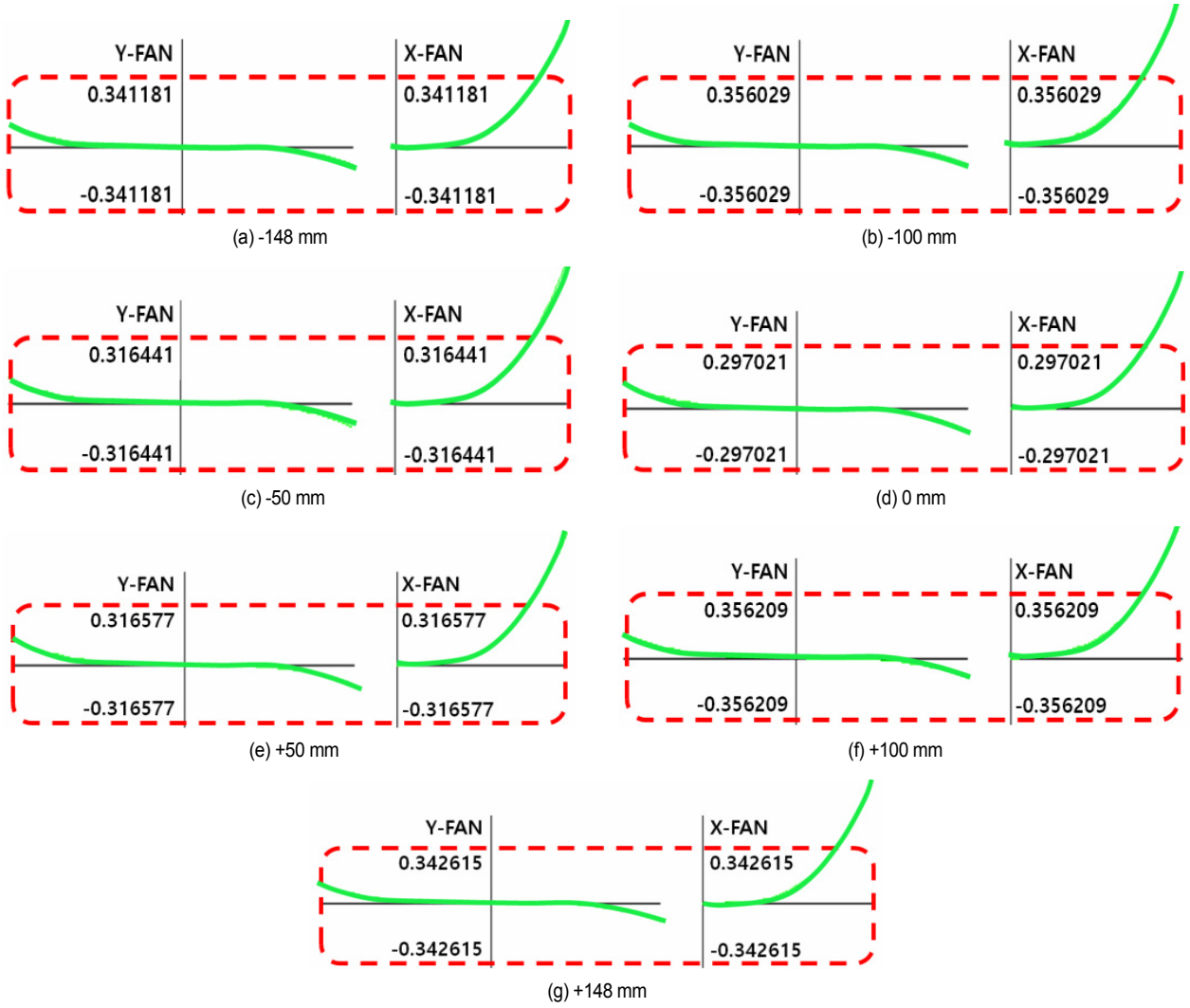

Fig. 5. Ray aberrations by location.

represents the exit surface radius of 43.439 mm; c and d represent the width of 14 mm and the thickness of 20 mm respectively.

$$F(H)=\frac{(Curv1)H^2}{1+\left(1-(1+K)(Curv1)^2H^2\right)^{1/2}}+(A)H^4 +(B)H^6+(C)H^8+(D)H^{10} \quad (1)$$

$$G(H)=\frac{(Curv2)}{1-(Curv2)F(H)} \quad (2)$$

$$Z(S,H)=F(H)\frac{G(H)S^2}{1+(1-G^2(H)S^2)^{1/2}} \quad (3)$$

$$Z=\frac{(Cx)X^2+(Cy)Y^2}{1+(1-(1+Kx)(Cx)^2X^2-(1+Ky)(Cy)^2Y^2))^{1/2}} +Ar((1-Ap)X^2+(1+Ap)Y^2)^2+Br((1-Bp)X^2+(1+Bp)Y^2)^3 +Cr((1-Cp)X^2+(1+Cp)Y^2)^4+Dr((1-Dp)X^2+(1+Dp)Y^2)^5. \quad (4)$$

3. Optical simulation and discussion

3.1 Simulation of laser printing and scanning unit

The previously designed laser printing and scanning unit optical system was applied into the optical simulation. Fig. 5 shows the photo aberration of the laser scanning unit by position (-148 mm to +148 mm) with (a) -148 mm in the y-x range of ±0.341181 mm; (b) -100 mm in the y-x range of ±0.356029 mm; (c) -50 mm in the y-x range of y-x ±0.316441 mm; (d) 0 mm in the y-x range of ±0.297021 mm; (e) +50 mm in the y-x range of ±0.316577 mm; (f) +100 mm y-x in the y-x range of ±0.356209 mm; (g) +148 mm in the y-x range of ±0.342615 mm. It was confirmed that the shape of the photo aberration was uniformly displayed in Fig. 5(g). Fig. 6 shows an optical system designed by simulating whether the point spread of the beam size has a constant magnitude for each section. As the results, the x-y coordinates point spread was measured as (a) 0.1078 mm at -148 mm; (b) 0.1114 mm at -100 mm; (c) 0.1099

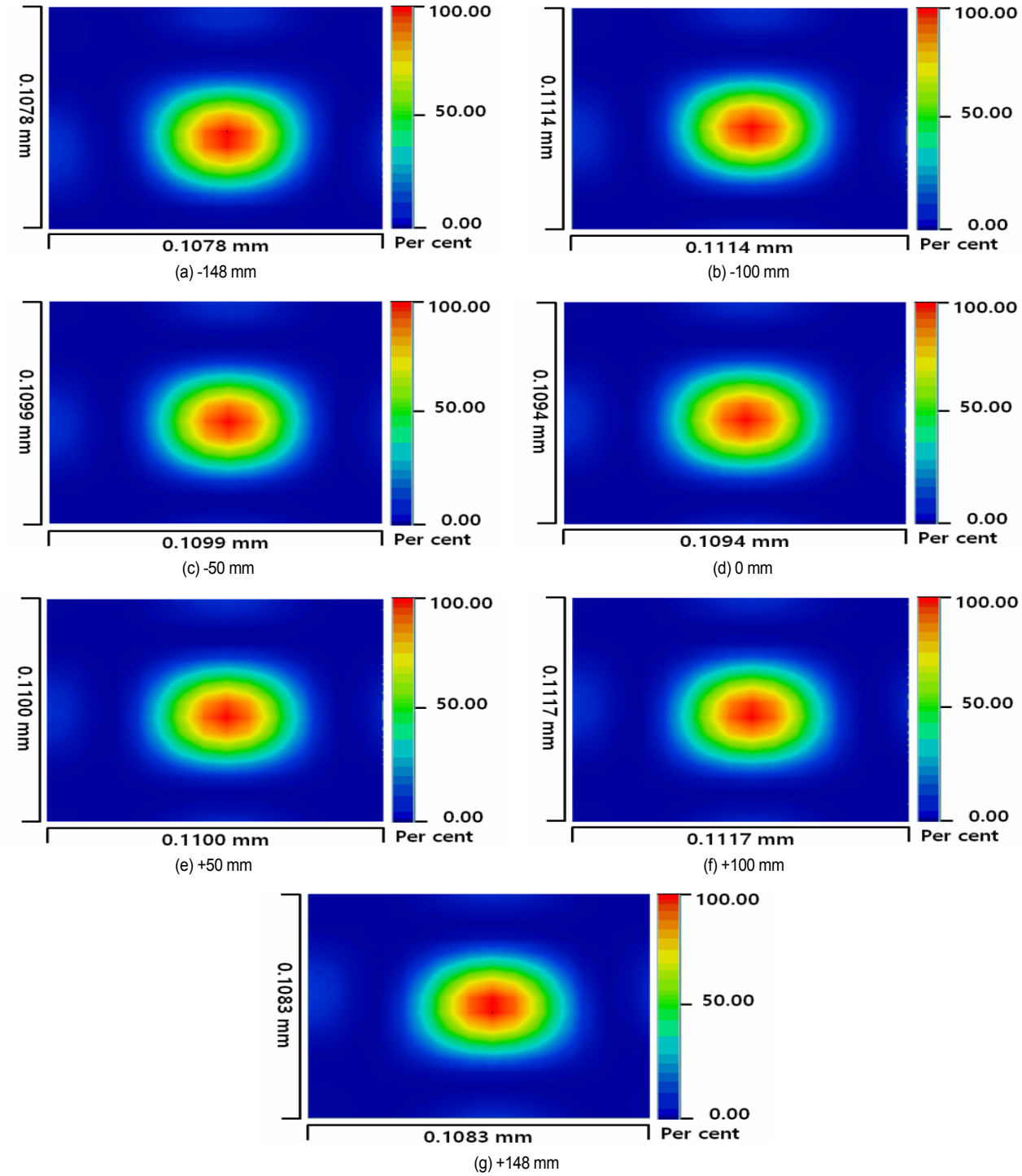

Fig. 6. Point spread function.

mm at -50 mm; (d) 0.1094 mm at 0 mm; (e) 0.1100 mm at +50 mm; (f) 0.1117 mm at +100 mm; (g) 0.1083 mm at +148 mm. It was confirmed that the point spread shape is displayed uniformly. Therefore, the goodness of ray aberration and beam size can be confirmed and the performance can be verified.

Fig. 7 shows the shape of the beam size as the spot diameter. When ray tracing is performed for each section, the shape of the actual beam passing through the image plane is verified. The optical system was designed and verified. With this process, it becomes possible to know which part of the f-theta lens passes. The problem in a specific part of the f-theta lens can be understand in this way. As shown in Fig. 8, the optical tolerance of such a laser printing and scanning unit was verified in the simulation process.

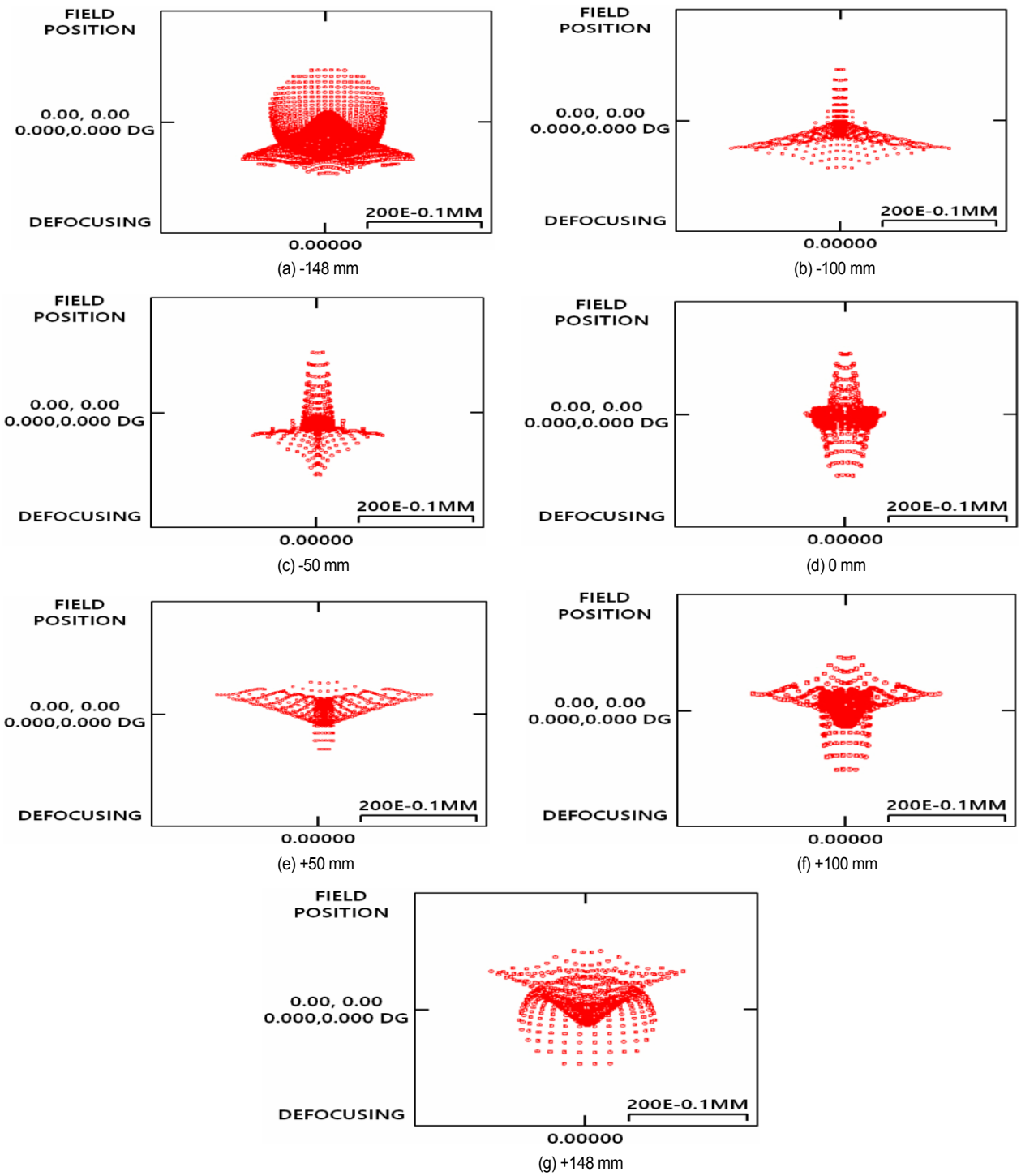

Fig. 7. Spot diameter.

3.2 Design and modeling of f-theta lens

Figs. 9(a) and (b) show the 2D drawing and 3D modeling of aspherical coefficients for f-theta lens design using optical design software (code-V). Table 5 shows the specifications of the entrance and exit surfaces of the effective surface of the f-theta lens.

4. Processing

4.1 Process of master f-theta lens

2D drawing and 3D modeling of design software were performed to process the master f-theta lens based on the designed optical system data. Based on the completed modeling data, roughing processing was performed using a high speed

Table 5. Effective surface drawing of the f-theta lens (code-V).

Item		Incident surface [mm]	Exit surface [mm]
Radius	Main scanning direction	553.367	-458.722
	Sub scanning direction	-458.722	-43.438
Radius tolerance		±6.3000	±4.0000
Clear aperture diameter		138.971	144.209
Edge diameter		149.344	
Edge diameter tolerance		0	
Thickness		20.000	
Thickness tolerance		±0.5000	

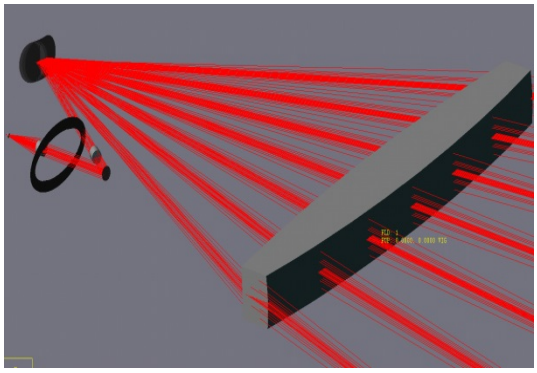

Fig. 8. Tolerance verification simulation.

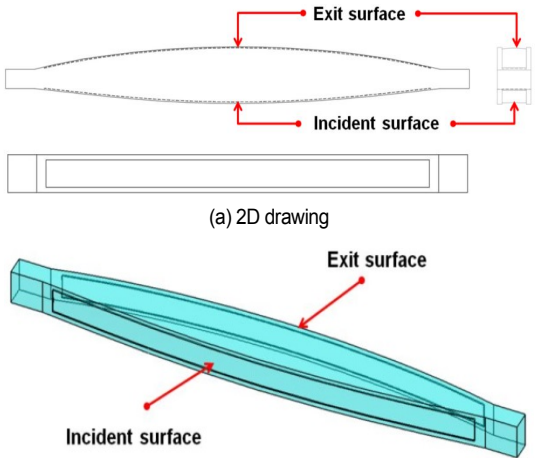

(a) 2D drawing

(b) 3D modeling

Fig. 9. Design of f-theta lens (code-V).

processing machine (Makino) during the primary processing. As the secondary processing, the master f-theta lens finishing was performed by using a special bite for processing f-theta lens as shown in Fig. 10. Fig. 11 shows a master f-theta lens that has been processed through repeated processes of roughing and finishing.

Fig. 10. Finish process of master f-theta lens.

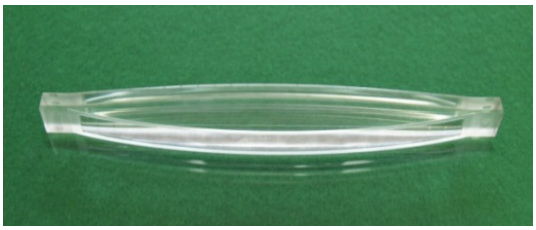

Fig. 11. Master f-theta lens.

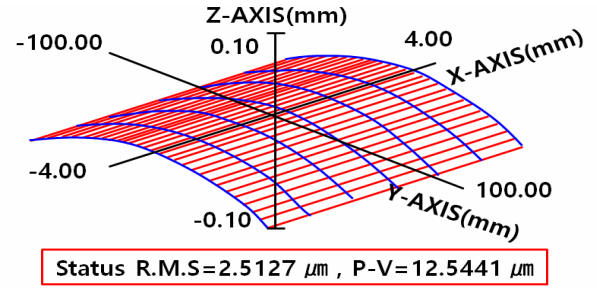

(a) Incident surface

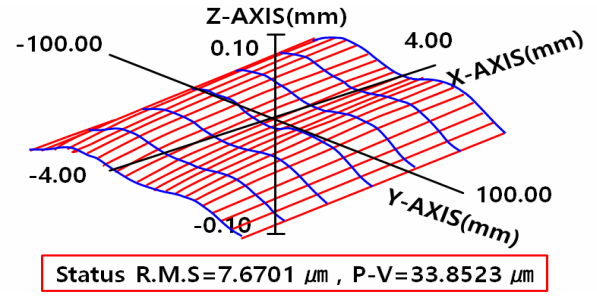

(b) Exit surface

Fig. 12. 1st result R.M.S and P-V of master f-theta lens using UA3P.

4.2 Experiments of master f-theta lens

The processed master f-theta lens was measured for surface roughness (root mean square) and surface shape accuracy (peak to valley) with a three-dimensional ultra-precision measuring device UA3P (UA3P: Panasonic). The measurement standard is based on a value that satisfies the surface roughness of 0.06 μm and the surface shape accuracy of 0.3 μm or less, which are the measurement standards of an aspherical lens. After the primary processing, as shown in Fig. 12, the measurement results show that the surface roughness of the incident surface is 2.5127 μm, the surface shape accuracy is

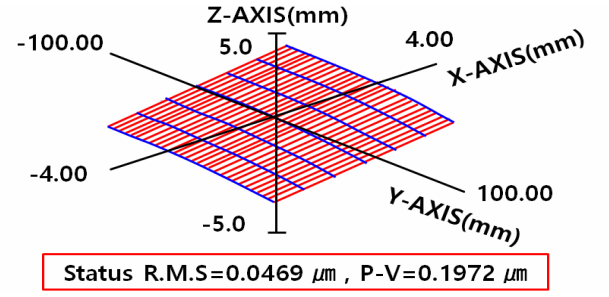

(a) Incident surface

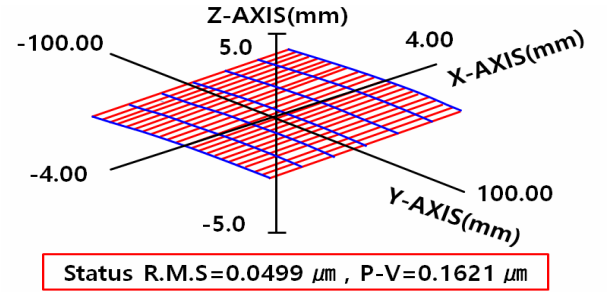

(b) Exit surface

Fig. 13. 2nd result RMS and P-V of master f-theta lens using UA3P.

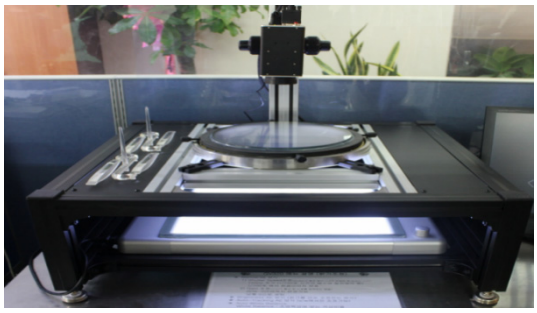

Fig. 14. Result double refraction machine.

12.5441 μm, the surface roughness of the exit surface is 7.6701 μm, and the surface shape accuracy is 33.8523 μm. These results are clearly more than the standard value. Unfortunately, the measurement result value was very unstable so the cutting tool used for roughing and finishing was modified and reworked. As shown in Fig. 13, the measurement results after the secondary processing show that the surface roughness of the incident surface is 0.0469 μm, the surface shape accuracy is 0.1972 μm, the surface roughness of the exit surface is 0.0469 μm, and the surface shape accuracy is 0.0499 μm. All were within the standard values and satisfactory measured values were obtained.

The processed master f-theta lens was checked for internal homogeneity with the birefringence checker in Fig. 14 in order to confirm the problems that occur during processing. To observe and confirm the quality of the processing, the finished master f-theta lens was checked for internal homogeneity with the birefringence tester as shown in Fig. 15. Fig. 16 shows the internal birefringence of the f-theta lens processing. (a) is a flat

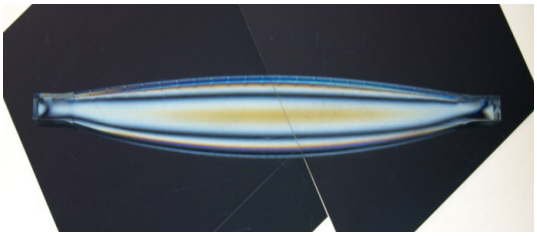

(a) Plane view

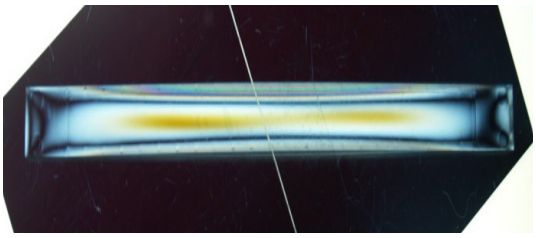

(b) Front view

Fig. 15. Result double refraction view of master f-theta lens.

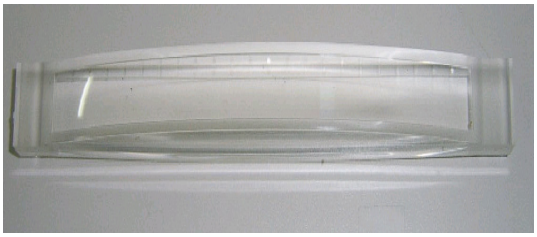

Fig. 16. Master f-theta lens.

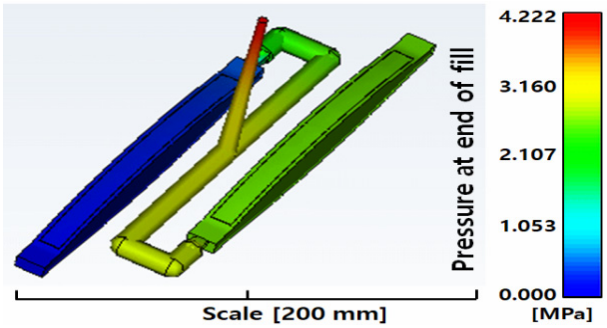

Fig. 17. Pressure required for injection molding of f-theta lens.

surface, and (b) is a front view. Cloudy areas, such as fog, have microbubbles formed inside, and the refraction of the beam transmitted through the f-theta lens is not smooth, causing performance to be not secured. Fig. 17 shows a master f-theta lens that has been completed by improving the birefringence shape by fine-correcting the birefringence state by heat.

4.3 Injection molding analysis

It is necessary to predict the internal and external aspects of the f-theta lens through CAE analysis to improve the optical performance, productivity, predict problems, and take countermeasures. Injection analysis was performed using analysis

Table 6. Injection molding conditions.

No.	Specification
Clamping force	140 Ton
Cavity number	1*2
Cavity weight	24.39 g
Resin	Zeonex e48r (cyclo olefin polymer)
Color	Optical
Drying temperature	90 °C
Filling time	17 sec
Cooling time	60 sec

software (Autodesk Moldflow Insight). The f-theta lens has a large number of elements in which stress is generated during the injection molding process. This causes a change in the internal physical property value. The optical characteristics of a lens are largely affected by two characteristics. These are the shape accuracy and internal physical characteristics. While the shape is being completed, the shape accuracy can be evaluated. However, the internal physical characteristics cannot be evaluated as such. This is because the performance of the optical component is affected as a whole by the distribution of stress in the internal physical property values during the progress of the injection process. Therefore, it is necessary to calculate the residual stress generated by filling, holding pressure, and cooling while also analyzing the optical verification characteristics that interfere with the optical performance. Before starting production of the lens, we attempted to confirm the fluidity of the molten resin in the mold so that the optical performance at the time of injection molding can be exhibited through injection molding analysis. It is possible to design this in advance to predict the mold ability, any defects in the product, check the design quality, reduce the number of mold modifications, and increase the production efficiency. Injection molding analysis has progressed to filling, leveling, and deformation analysis, and the material used was Zeonex e48r(Cyclo olefin polymer), which is a resin with excellent optical properties. The process conditions for injection molding are shown in Table 6.

Injection molding analysis of the f-theta lens can grasp the flow of the resin fluid which determines the size and structure of the sprue and runner, thus optimizing resin flow and forming the mold. The pressure required to eject the f-theta lens is shown in Fig. 17, the maximum is 4.222 MPa and the filling time appears after 27 sec for injection molding is shown in Fig. 18. The quality level of injection molding showed an excellent filling ability can be observed in Fig. 19. The filling analysis result shows that the filling was done without unmolded areas and the entrance and exit surfaces of the lens finished at the same time. Simulations confirmed that there was no problem with the balance. For the production of injection molding of f-theta lens, it was possible to use a 140 Ton electric injection machine which simulated that an injection could be performed in a 2 cavity mold production with an injection pressure of

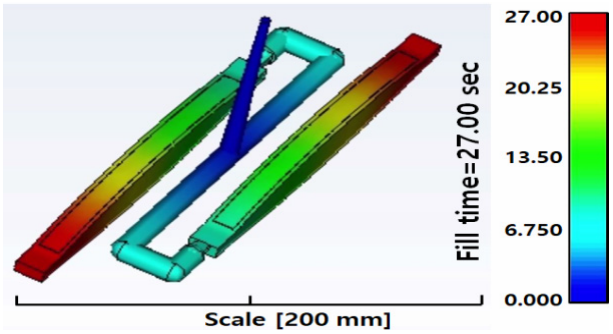

Fig. 18. Filling time required for injection molding of f-theta lens.

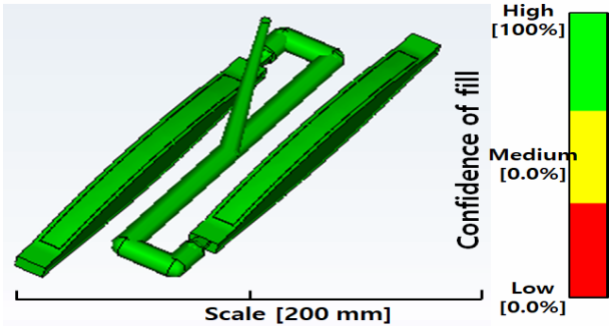

Fig. 19. Injection molding filling rate of f-theta lens.

90 MPa and a mold clamping force of 140 Ton.

5. Conclusions

In this research, we studied the design and production of the f-theta lens of the laser printing and scanning unit. The optical characteristics of the f-theta lens were confirmed in the 600 dpi f-theta lens design and simulation of the laser printing and scanning unit. The optical performance of the master f-theta lens on the effective surface was confirmed through precision high-speed machining and ultra-precision machining with the laser printing and scanning unit's 600 dpi master f-theta lens machining. The filling and pressure simulation of the f-theta lens injection process of the laser printing and scanning unit was performed. Based on such data, it will be possible to improve the performance and mass productivity of the f-theta lens and laser printing and scanning unit in the future.

1) It was found that the optical path difference was good in the simulation of discrimination from -148 mm to +148 mm because the design data of the optical system of the laser printing and scanning unit could be emitted.

2) The beam size was expressed by the shape of the point spread function in the optical system of the laser printing and scanning unit. It was found that a certain shape and size are implemented for beam size confirmation from -148 mm to +148 mm.

3) With the optical system of the laser printing and scanning unit, it was possible to know the shape of the beam passing through the image plane in the interval of -148 mm to +148 mm

with the diameter shape of the point by simulation.

4) The surface roughness of the incident surface of the maser f-theta lens is 0.0469 μm and the surface shape accuracy is 0.772 μm. The surface roughness is 0.06 μm, which is the standard value for aspherical lenses, and the surface shape accuracy is within 0.3 μm. I was satisfied with these values.

5) The surface roughness of the exit surface of the master f-theta lens is 0.0499 μm and the surface shape accuracy is 0.1621 μm. The surface roughness is 0.06 μm, which is the standard value for aspherical lenses, and the surface shape accuracy is within 0.3 μm. I was satisfied with these values.

6) It was found that the birefringence shape of the master f-theta lens can be corrected by heat to improve performance.

7) The maximum pressure required for injection molding of the f-theta lens was 4.222 MPa, and the quality level of injection molding could be known by simulation.

8) The f-theta lens was filled during injection molding for 27 sec of injection time without the rice molding area because the filling was performed at the same time on both the entrance surface and the exit surface of the lens. I was able to know by simulation that there was no balance problem.

Acknowledgments

This study was supported by the Basic Science Research Program through the NRF of Korea (NRF) funded by the MEST (NRF-2020R1A2C1011958).

References

[1] H. Takanori, M. Takesuke, I. Hisao, D. Masaharu and A. Yoshio, Laser scanning optical system with plastics lenses featuring high resolution, *Proc. of SPIE*, 1670 (1992) 404-415.

[2] B. Kim, J. K. Kim, C. K. Park, S. K. Oh, S. B. Kim, S. Kim and J. Lim, Design and fabrication of concentrated photovoltaic optics with high numerical aperture using a curved catadioptric optical system, *J. Mech. Sci. Technol.*, 30 (3) (2016) 1315-1322.

[3] D. Y. Zhang, V. Lien, Y. Berdichevsky, J. Choi and Y. H. Lo, Fluidic adaptive lens with high focal length tunability, *American Institute of Physics,* 82 (19) (2003) 3171-3172.

[4] R. J. Bensingh, S. R. Boopathy and C. Jebaraj, Minimization of variation in volumetric shrinkage and deflection on injection molding of Bi-aspheric lens using numerical simulation, *J. Mech. Sci. Technol.*, 30 (11) (2016) 5143-5152.

[5] Y. J. Chang, C. K. Yu, H. S. Chiu, W. H. Yang, H. E. Lai and P. J. Wang, Simulations and verifications of true 3D optical parts by injection molding process, *Proc. of ANTEC*, 22 (2009) 253-258.

[6] G. H. Hu and Z. S. Cui, Effect of packing parameters and gate size on shrinkage of aspheric lens parts, *J. of Shanghai Jiaotong Univ.*, 15 (2010) 84-87.

[7] W. Michaeli, S. Hebner, F. Klaiber and J. Forster, Geometrical accuracy and optical performance of injection moulded and injection-compression moulded plastic parts, *CIRP Annals - Manufacturing Technology,* 56 (2007) 545-548.

[8] Y. Zhang, B. Zhao, Y. Wang and F. Chen, Effect of machining parameters on the stability of separated and unseparated ultrasonic vibration of feed direction assisted milling, *J. Mech. Sci. Technol.*, 31 (2) (2007) 851-858.

[9] E. Baburaj, K. M. M. Sundaram and P. Senthil, Effect of high speed turning operation on surface roughness of hybrid metal matrix (Al-SiCp-fly ash) composite, *J. Mech. Sci. Technol.*, 30 (1) (2016) 89-95.

[10] H. S. Park and X. P. Dang, Optimization of conformal cooling channels with array of baffles for plastic injection mold*, Int. J. Precis. Eng. Manuf.,* 11 (2010) 879-890.

[11] G. Klepek, Manufacturing optical lens by injection compression molding, *Kunststoffe,* 77 (1987) 13.

[12] Y. B. Lee, T. H. Kwon and K. Yoon, Numerical prediction of residual stresses and birefringence in injection/compression molded center-gated disk, part 2: Effects of processing conditions, *Polym. Eng. Sci.,* 42 (2002) 2273-2292.

[13] S. C. Chen, Y. C. Chen and N. T. Cheng, Simulation of injection compression mold-filling process, *Int. Comm. Heat Mass Transfer,* 25 (1998) 907-917.

[14] M. J. Noh, D. H. Hyun, H. S. Chang, Y. W. Park and C. Y. Park, System design for laser scanning unit using A3, *Journal of the Korean Society of Manufacturing Technology Engineers*, 11 (2011) 71-72.

[15] K. S. Yoo, D. H. Hyun, H. S. Chang, Y. W. Park and C. Y. Park, Injection molding of a laser scanning unit optical system, *Journal of the Korean Society of Manufacturing Technology Engineers,* 11 (2011) 102-103.

[16] C. S. Lim, The effect analysis of birefringence of plastic f-theta lens on the beam diameter, *Korean Journal of Optics and Photonics,* 11 (2000) 73-79.

[17] K. Park and C. Y. Han, Numerical analysis for the injection molding of an aspheric lens for a photo pick-up device, *Journal of the Korean Society of Precision Engineering,* 21 (2004) 163-170.

[18] D. K. Lee, Y. S. Yang, S. S. Kim, H. J. Kim and J. H. Kim, Development of F theta lens for laser scanning unit, *Journal of the Korean Physical Society,* 53 (2008) 2527-2530.

[19] D. H. Lee and S. H. Park, Design and development of F-theta lens for 1064 nm laser, *Journal of Korean Ophthalmic Opt. Soc.,* 21 (2016) 401-407.

[20] I. S. Jeong, M. S. Ban, K. E. Son and B. B. Lee, Development of F-theta lens for laser scanning unit, *Trans. Korean Soc. Mech. Eng. C,* 1 (2013) 13~19.

[21] K. Park and C. Y. Han, Numerical analysis for the injection molding of an aspheric lens for a photo pick-up device, *Journal of the Korean Society of Precision Engineering,* 21 (2004) 163-170.

[22] R. D. Bringans, Application of blue diode lasers to printing*, Proc. of Materials Research Society Symposium,* 482 (1998) 1203-1210.

[23] K. H. Ye and H. W. Choi, Laser head design and heat transfer Analysis for 3D patterning, *Journal of the Korean Society of Manufacturing Process Engineers,* 15 (2016) 46-50.

[24] L. Carmina, T. P. William and P. C. Peter, Athermalization of a single-component lens with diffractive optics, *Applied Optics,* 32 (1993) 2295-2302.

[25] M. Kazuo, Historical review and future trends of scanning optical systems for laser beam printers, *Proc. of SPIE,* 1987 (1993) 264-273.
[26] S. Y. Kim, B. G. Park, J. O. Jung, K. S. Cho and I. S. Chung, Metal injection molding analysis for developing embroidering machine rotary hooks, *Journal of the Korean Society of Manufacturing Process Engineers,* 17 (2018) 160-168.
[27] C. Donald, J. Thomas, D. Alan and W. Dennis, *Diffractive Optics: Design, Fabrication, and Test*, SPIE Press (2003) 57-82.

Yong-Woo Park is a Ph.D. candidate in the Department of Convergence Mechanical Engineering, Gyeongsang National University. His research interest is Mechanical System Design.

Zhen Qin received the B.E. degree from Gachon University, Seongnam, Korea in 2013. He received his M.S. and Ph.D. degrees in mechanical and aerospace engineering from Gyeongsang National University, Jinju, Korea, in 2019 and 2021, respectively. He has worked at R&D center of Kdac Co., Ltd., since 2013. Dr. Qin is currently a Professor of Shandong University of Technology in Zibo, China.

Sung-Ki Lyu received his bachelor's, master's degrees at Chonbuk National University, Korea, in 1987 and 1989, respectively. And he got the doctor's degrees at Tohoku University, Japan, in 1994. Dr. Lyu is currently a Professor of Gyeongsang National University in Jinju, Korea.